Flatness-based control of a two-degree-of-freedom platform with pneumatic artificial muscles

David Bou Saba, Paolo Massioni, Eric Bideaux, Xavier Brun

Flatness-based control of a two-degree-of-freedom platform with pneumatic artificial muscles

David Bou Saba
Laboratoire Ampère CNRS,
INSA Lyon, Université de Lyon,
69621 Villeurbanne CEDEX, France
Email: david.bou-saba@insa-lyon.fr

Paolo Massioni
Laboratoire Ampère CNRS,
INSA Lyon, Université de Lyon,
69621 Villeurbanne CEDEX, France
Email: paolo.massioni@insa-lyon.fr

Eric Bideaux
Laboratoire Ampère CNRS,
INSA Lyon, Université de Lyon,
69621 Villeurbanne CEDEX, France
Email: eric.bideaux@insa-lyon.fr

Xavier Brun
Laboratoire Ampère CNRS,
INSA Lyon, Université de Lyon,
69621 Villeurbanne CEDEX, France
Email: xavier.brun@insa-lyon.fr

Pneumatic artificial muscles are an interesting type of actuators as they provide high power-to-weight and power-to-volume ratio. However, their efficient use requires very accurate control methods taking into account their complex and nonlinear dynamics. This paper considers a two-degree-of-freedom platform (a simplified version of a Stewart platform) whose attitude is determined by three pneumatic muscles controlled by servovalves. An overactuation is present as three muscles are controlled for only two degrees of freedom. The contribution of this work is twofold. First, whereas most of the literature appraches the control of systems of similar nature with sliding mode control, we show that the platform can be controled with the flatness-based approach by chosing an appropriate flat output. This method is a non-linear open-loop controller introduced by Fliess et al. [1]. In addition, this approach is model-based, and it can be applied thanks to the very accurate models of the muscles, the platform and the servovalves that have been recently experimentally developed. Second, we solve the overactuation of the platform, by an adequate choice for the range of the efforts applied by the muscles. In this paper, we recall the basics of this control technique and then show how it is applied to the proposed experimental platform. In addition to the flatness-based controller, a proportional-integral controller is added in order to overcome the modeling errors. At the end of the paper, the proposed approach is compared to the most commonly used control method, and its effectiveness is shown by means of experimental results.

Nomenclature

P_0 Atmospheric pressure.
θ_0 Weave angle of the muscle at rest.
D_0 Diameter of the muscle at rest.
l_0 Length of the muscles at rest.
α Experimentally determined power coefficient.
K Experimentally determined coefficient.
ε_a Experimentally determined coefficient.
ε_b Experimentally determined coefficient.
k Polytropic index (air).
r Perfect gas constant.
T Air temperature.
R Muscle application point distance from center (constant).
J Momentum of inertia about an horizontal axis (constant).
$\phi_1 = -90^\circ$ Angular position of the 1st muscle (constant).
$\phi_2 = 30^\circ$ Angular position of the 2nd muscle (constant).
$\phi_3 = 150^\circ$ Angular position of the 3rd muscle (constant).
θ_x Angular position of the platform around x axis.
θ_y Angular position of the platform around y axis.
P_i Absolute pressure inside the i^{th} muscle.
v_i Voltage applied to the i^{th} servovalve.
V_i Volume of the i^{th} muscle.
q_i Mass flow into the i^{th} muscle.
ε_i Contraction of the i^{th} muscle.
ε_0 Initial contraction of the muscle.
F_i Force applied by the i^{th} muscle.
Γ Perturbation torques.

1 Introduction

Pneumatic artificial muscles (PAMs) are an efficient type of actuators featuring high power-to-volume ratio and high pulling efforts at a relatively low price. [2,3] This makes their use quite interesting in many engineering and robotic applications, even if their control is problematic due to the non-linearity found in their behavior.

The control of PAMs has been approached with several methods trying to cope with the strong nonlinearities of their dynamics. The approaches found in the literature are mainly inherently nonlinear control methods; [4, 5] sliding mode controllers are one of the most common choices, [6, 7, 8] also sometimes combined with adaptive or neural controllers, [9, 10, 11] or backstepping. [12] Sliding mode controllers in fact provide enough robustness with respect to a dynamical model containing uncertainties. Nonetheless, the main drawback of the sliding mode control is the chattering phenomenon (quick switching of the control action).

The nonlinearity in the model of the pneumatic muscles stems from the fact that the contraction effort they produce is a nonlinear function of both internal pressure and relative length contraction (as shown in Fig. 3). Some hysteresis effects can also be remarked as the effort produced is not the same if the muscle is being contracted or deflated. The models of PAMs reported in the literature either do not take into consideration this phenomenon when designing the control law, or consider it as a model uncertainty. It is noteworthy to mention that while many models of PAMs can be found [2, 13, 14], the model we adopt in this work is a new, experimentally obtained model [15] resulting from static and dynamic tests done at our laboratory. These tests have provided a very accurate model for the specific PAM that we consider in this work. As observed experimentally, the hysteresis phenomenon is relatively small and can be approximated by the average of the values obtained in both compression and deflation at each working point of the muscle. It is worth mentioning that other references have adopted other (possibly more complicated) approaches to solve this issue, see for instance Schindele et al. [16].

The topic of this paper is a study of a two-degree-of-freedom platform, actuated by three pneumatic muscles. The objective is the synthesis of a model-based control law allowing the tracking of a reference trajectory for a wide operating range of the muscles. The platform is constrained to a limited operating domain due to mechanical constraints and to the fact that the muscles generate only pulling forces. Furthermore, the system can be considered as overactuated (three actuators moving two degrees of freedom), which requires a control allocation strategy.

In this work, we propose a flatness-based (feedforward) control [1] that simultaneously exploits the model of all the elements involved and solves the over-actuation problem. The originality of adopting this model-based approach lies in the very detailed and recently developed experimental models of the muscles, that together with the inherently nonlinear control method, lead to a high accuracy in the trajectory tracking for a wide range of set-points. Furthermore, we provide a theoretical proof of the flatness of the system by considering a flat output that also allows an allocation control strategy. The robustness with respect to model errors is provided by coupling the flatness-based controller with a proportional-integral (PI) controller feeding back the error with respect to the reference trajectory.

The paper is structured as follows. At first, we introduce the notation used throughout the paper. Subsequently, we introduce the model of the platform and of all its elements, including the pneumatic artificial muscles. We then show that a proper choice of outputs makes the system flat, and therefore a flatness-based control law is possible. Afterwards, the problem of overactuation is studied. At last, some experimental results are shown before concluding.

2 Notations and definitions

Let $\mathbb{R}$ be the set of real numbers, and $\mathbb{N}$ the set of the strictly positive integers. For a matrix A, $A^\top$ denotes the transpose of A. Given two functions $f(x), g(x) \in \mathbb{R}^n$, with

$x \in \mathbb{R}^n$, let the Lie derivative of f along g be defined as $L_g f(x) = \frac{\partial f(x)}{\partial x} \cdot g(x)$. For $\xi \in \mathbb{N}$, let $L_g^{\xi} f(x) = \frac{\partial L_g^{\xi-1} f(x)}{\partial x} \cdot g(x)$, with $L_g^0 f(x) = f(x)$. For all signals x depending on the time t, $x^{(\xi)}$ will indicate its ξ-th time derivative, i.e. $x^{(1)} = \frac{dx}{dt} = \dot{x}$, $x^{(2)} = \frac{d^2x}{dt^2} = \ddot{x}$, etc.

All the symbols concerning the pneumatic muscle platform are defined in the nomenclature section.

3 The pneumatic platform

3.1 Description

The pneumatic platform studied in this paper is represented in Fig. 1 and Fig. 2. It consists of a metal plate fixed to a central spherical hinge on top of a vertical beam, with three pneumatic muscles (Festo DSMP), controlled by servovalves Festo MPYE-5-M5-010-B, attached radially to the plate at equally spaced points. Due to the structure of the system and since the muscles can only exert pulling efforts in the same direction of their central axis (which is assumed to be vertical in our case), the motion of the platform will be restricted to only two degrees of freedom, i.e. the two rotational angles (θ_x and θ_y) with respect to horizontal axes passing through the hinge. An inclinometer (TE Connectivity G-NSDOG2-001) provides the measurement of these angles, and pressure sensors (Festo SDET-22T-D10-G14-U-M12) are present at each muscle. The sensors and acuators are connected to a computer through a dSPACE system.

This platform can be considered as a simplified version of a Stewart platform. Therefore, it is a test bench on which control laws can be tried and evaluated before moving to more complex systems with more degrees of freedom.

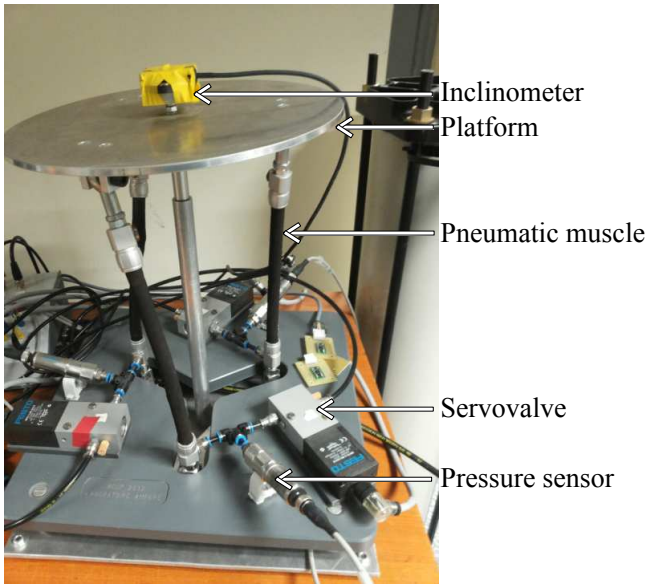

Fig. 1. The experimental platform.

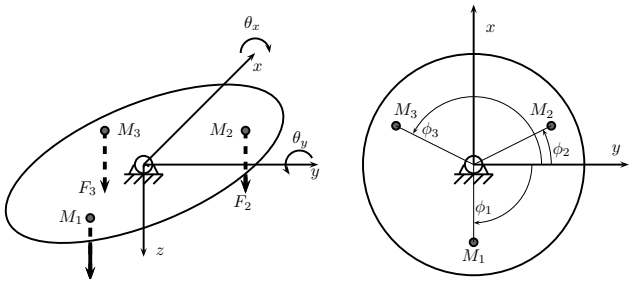

Fig. 2. Axonometric view and view from the top of the top plate, with definition of the axes x, y, z and the rotation angles θ_x and θ_y. M_1, M_2 and M_3 are the attachment points of the three pneumatic artificial muscles and define the three angular positions ϕ_1, ϕ_2 and ϕ_3 given in the nomenclature section.

3.2 Model

This section reports the differential equations describing the system dynamics and the different assumptions made. A more detailed description of the complete model of the system is presented in Bou Saba et al. [17], with all the hypotheses and explanations. The interested reader may refer as well to Sermeno Mena et al. [15] for more details (including how the hysteresis has been approximated) about the experiments made on the PAM model we adopt.

The first elements to be modeled are the pneumatic muscles, which are supposed to be identical (they have the same length at rest l_0, the same initial contraction ε_0, etc.). The length contraction of each muscle ($i \in \{1,2,3\}$) can be written as:

$$\varepsilon_i = \frac{R}{l_0}\left(\cos\phi_i \sin\theta_y - \sin\phi_i \sin\theta_x \cos\theta_y\right) + \varepsilon_0. \qquad (1)$$

Subsequently, the rate of contraction of each muscle is the time derivative of ε_i, i.e.

$$\dot{\varepsilon}_i = \frac{R}{l_0}\left[-\dot{\theta}_x \sin\phi_i \cos\theta_x \cos\theta_y + \dot{\theta}_y\left(\cos\phi_i \cos\theta_y + \sin\phi_i \sin\theta_x \sin\theta_y\right)\right]. \qquad (2)$$

The direct dynamical model [17] is written as

$$\begin{bmatrix}\ddot{\theta}_x \\ \ddot{\theta}_y\end{bmatrix} = M\left(\theta_x, \theta_y\right)\begin{bmatrix}F_1 \\ F_2 \\ F_3\end{bmatrix} + \frac{1}{J}\Gamma \qquad (3)$$

where the matrix $M\left(\theta_x, \theta_y\right)$ is given in equation (4) at the top

$$M(\theta_x,\theta_y)=\frac{R}{J}\begin{bmatrix} -\sin\phi_1\cos\theta_x\cos\theta_y & -\sin\phi_2\cos\theta_x\cos\theta_y & -\sin\phi_3\cos\theta_x\cos\theta_y \\ \cos\phi_1\cos\theta_y+\sin\phi_1\sin\theta_x\sin\theta_y & \cos\phi_2\cos\theta_y+\sin\phi_2\sin\theta_x\sin\theta_y & \cos\phi_3\cos\theta_y+\sin\phi_3\sin\theta_x\sin\theta_y \end{bmatrix} \tag{4}$$

$$\begin{cases} E(\theta_x,\theta_y)=\dfrac{R}{J}\begin{bmatrix} -\sin\phi_1\cos\theta_x\cos\theta_y & -\sin\phi_2\cos\theta_x\cos\theta_y \\ \cos\phi_1\cos\theta_y+\sin\phi_1\sin\theta_x\sin\theta_y & \cos\phi_2\cos\theta_y+\sin\phi_2\sin\theta_x\sin\theta_y \end{bmatrix} \\ G(\theta_x,\theta_y)=\dfrac{R}{J}\begin{bmatrix} -\sin\phi_3\cos\theta_x\cos\theta_y \\ \cos\phi_3\cos\theta_y+\sin\phi_3\sin\theta_x\sin\theta_y \end{bmatrix} \end{cases} \tag{5}$$

of the next page. The term $\Gamma=[\Gamma_x,\Gamma_y]^\top$ contains the torques that will not be modeled (as an arbitrary choice) and will be left to the feedback control to take care of. Such terms are either due to friction, or to gyroscopic couplings between the two axes, or to external forces acting on the platform. The friction terms are quite difficult to model exactly, whereas the gyroscopic couplings are relatively small due to the fact that the platform keeps always almost horizontal and moves at relatively low angular velocities. This allows considering the platform's movement around each axis as decoupled, according to (3) above. Such an equation can also be written as

$$\begin{bmatrix}\ddot{\theta}_x\\ \ddot{\theta}_y\end{bmatrix}=E(\theta_x,\theta_y)\begin{bmatrix}F_1\\F_2\end{bmatrix}+G(\theta_x,\theta_y)F_3+\frac{1}{J}\Gamma \tag{6}$$

where the matrices $E(\theta_x,\theta_y)$ and $G(\theta_x,\theta_y)$ are given in equation (5) at the top of the next page. This form separates the effect of the first two forces with respect to F_3, which makes it easier to approach the overactuation problem.

In turn, the effort exerted by a pneumatic muscle can be modeled with a quasi-static model [17, 15] as

$$F_i(P_i,\varepsilon_i)=H(\varepsilon_i)(P_i-P_0)+L(\varepsilon_i), \tag{7}$$

where

$$H(\varepsilon_i)=\frac{\pi D_0^2}{4}\left[\frac{3(1-\varepsilon_i)^\alpha}{\tan^2\theta_0}-\frac{1}{\sin^2\theta_0}\right], \tag{8}$$

$$L(\varepsilon_i)=K\frac{\varepsilon_i(\varepsilon_i-\varepsilon_a)}{\varepsilon_i+\varepsilon_b}, \tag{9}$$

and α, K, ε_a and ε_b experimentally determined constants [15]. Considering that the operating range of the servovalves is 1.25 bar $\leqslant P_i \leqslant$ 7 bar, the contraction force in the operating domain for each muscle is represented in Fig. 3. Only contraction forces are possible (the muscles cannot push), therefore $F_i \geqslant 0$.

Notice that the angles of the platform (θ_x, θ_y) are physically constrained to be in the range $[-15°, 15°]$. Accordingly, contractions ε_i are within the range $[-0.03, 0.21]$, for which $H(\varepsilon_i)$ is never equal to 0.

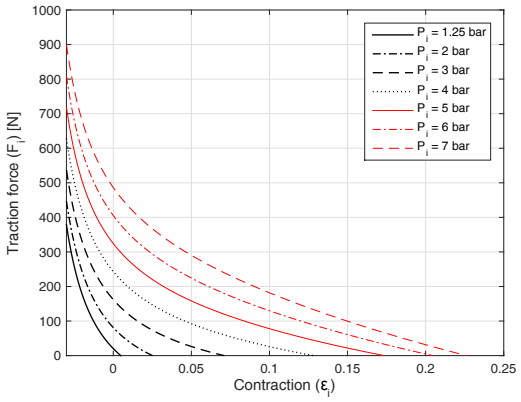

Fig. 3. Contraction force applied by a muscle as a function of the contraction ε_i and absolute pressure P_i.

The pressure inside each muscle is modeled as

$$\dot{P}_i=\frac{krT}{V_i(\varepsilon_i)}\left[q_i(P_i,v_i)-\frac{P_i}{rT}\frac{\partial V(\varepsilon_i)}{\partial\varepsilon_i}\dot{\varepsilon}_i\right] \tag{10}$$

where k is the polytropic index of the gas, r the perfect gas constant, T the temperature, q_i the mass flow of gas, and V_i the volume of the muscle, for which the following formula has been proposed [17, 15]

$$\frac{\partial V}{\partial \varepsilon_i}(\varepsilon_i) = \frac{\pi}{4} D_0^2 l_0 \left[-\frac{1}{\sin^2 \theta_0} + (\alpha+1)\frac{(1-\varepsilon_i)^\alpha}{\tan^2 \theta_0} \right]. \quad (11)$$

The parameters D_0, l_0 and θ_0 are defined in the nomenclature section. The temperature T is considered constant, due to the fact that the relative variation of the temperature during the movement of the muscle is very low and thus neglected for simplicity.

At last, the mass flow of gas q_i entering each muscle is a nonlinear function of the pressure inside the muscle and the voltage v_i fed to the servovalve. More precisely, it can be modeled [18] as:

$$q_i(v_i, P_i) = \varphi(P_i) + \psi(P_i, \mathrm{sgn}(v_i))v_i \quad (12)$$

where φ and ψ are two invertible polynomial functions with a minimal degree of 4 and 5 respectively. The coefficients of the polynomial functions have been determined numerically by approximation of the experimental data obtained by our research group at the Ampère laboratory. [18] This function is graphically depicted in Fig. 4. We note as well that the dynamical model of the servovalve is neglected due to its very fast dynamics and large pass-band ($\sim$ 100 Hz) compared to the dynamics of platform and muscles ($\sim$ 1 Hz).

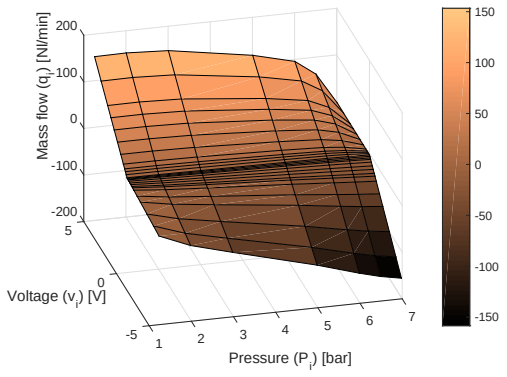

Fig. 4. Mass flow of a servovalve as a function of voltage v_i and absolute muscle pressure P_i.

Note that from equation (12) and because of the invertibility of φ and ψ, the model of the servovalve is invertible, i.e. we can always find the required voltage v_i that should be applied to the i^{th} servovalve in order to have a desired flow q_i for a defined pressure P_i in the i^{th} muscle. The inverse of this model will be used in the control synthesis.

3.3 Control objectives

The aim of this test rig is to demonstrate the ability to track any smooth trajectory of θ_x and θ_y. Trajectories of this kind can be chosen as infinitely differentiable piece-wise functions without loss of generality in the control synthesis.

4 Model analysis and control

The accurate modeling, previously proposed, enables proper application of non-linear control theory, such as flatness-based control. Before being applicable, an essential condition has to be verified; it consists in proving that the system is flat. The relevant concepts about flatness are recalled here.

4.1 Flatness and flatness-based control

The concept of flat system and flatness-based control for nonlinear systems have been introduced in Fliess et al. [1] Basically, the "flatness" is a property of a dynamical system and a choice of its output y, as defined here.

Definition 1 (Flat system [1, 19]). *A dynamical system of equations*

$$\dot{x} = f(x) + g(x)u \quad (13)$$

with $x \in \mathbb{R}^n$, $u \in \mathbb{R}^m$ is flat if and only if there exist an $\mathbb{R}^m$-valued smooth function h depending on x and a finite number $\mu \in \mathbb{N}$, such that the square differential-algebraic system defined by (13) and the by the following equation

$$y = h(x, u, u^{(1)}, \ldots, u^{(\mu)}) \quad (14)$$

has a solution (x,u) of the form

$$x = \eta(y, y^{(1)}, \ldots, y^{(\nu-1)}), \quad (15)$$

$$u = \xi(y, y^{(1)}, \ldots, y^{(\nu)}), \quad (16)$$

for an appropriate value of $\nu \in \mathbb{N}$, where η and ξ are smooth functions in $\mathbb{R}^n$ and $\mathbb{R}^m$ respectively. The output y is then called "flat output".

The idea of flatness can be explained briefly as follows. If one can choose as many output variables y_i as inputs (the system is square), in a way to recover the state and the inputs from these output variables and their successive derivatives, then the system is flat and a flatness-based, open-loop control law can be derived by system inversion (as applied later on). The subtlety in this task lies in the capability of expressing every state variable and input variable **independently** as functions of the output variables and their successive derivatives. Two fundamental concepts for system inversion are the relative degree and the coupling matrix.

Definition 2 (Relative degree). *The relative degree of the i^{th} component y_i of y is the smallest $\rho_i \in \mathbb{N}$ for which $L_{g_j} L_f^{\rho_i - 1} h_i \neq 0$ for at least one value of j, $j \in \{1, \cdots, m\}$. The relative degree will determine how many times an output has to be differentiated in order to get to a corresponding input variable.*

Definition 3 (Coupling matrix). *The coupling matrix $\Delta(x)$ is given by the expression:*

$$\Delta(x) = \begin{bmatrix} L_{g_1} L_f^{\rho_1 - 1} h_1 & L_{g_2} L_f^{\rho_1 - 1} h_1 & \dots & L_{g_m} L_f^{\rho_1 - 1} h_1 \\ L_{g_1} L_f^{\rho_2 - 1} h_2 & L_{g_2} L_f^{\rho_2 - 1} h_2 & \dots & L_{g_m} L_f^{\rho_2 - 1} h_2 \\ \vdots & \vdots & \ddots & \vdots \\ L_{g_1} L_f^{\rho_m - 1} h_m & L_{g_2} L_f^{\rho_m - 1} h_m & \dots & L_{g_m} L_f^{\rho_m - 1} h_m \end{bmatrix}. \quad (17)$$

Differentiating (14) with respect to time and using (13), we have that

$$\begin{bmatrix} y_1^{(\rho_1)} \\ y_2^{(\rho_2)} \\ \vdots \\ y_m^{(\rho_m)} \end{bmatrix} = \Delta(x) u + \begin{bmatrix} L_f^{\rho_1} h_1 \\ L_f^{\rho_2} h_2 \\ \vdots \\ L_f^{\rho_m} h_m \end{bmatrix}. \quad (18)$$

The control law which has been applied to the test rig is based on the following theorem, which is a well-known result for which no proof is necessary here.

Theorem 1. *(Proposition 4 From Fliess et al. [1]) If a system of equations $\dot{x} = f(x) + g(x)u$ with $u \in \mathbb{R}^m$ is flat (Definition 1) with respect to a flat output $y = h(x) \in \mathbb{R}^m$ with relative degrees ρ_i, then the system is controllable.*

Therefore, for a flat (thus controllable) system, an explicit control law can be found by inverting equation (18). Consequently, the following open-loop law

$$u = \Delta(x)^{-1} \left(\begin{bmatrix} y_{1,\mathrm{ref}}^{(\rho_1)} \\ y_{2,\mathrm{ref}}^{(\rho_2)} \\ \vdots \\ y_{m,\mathrm{ref}}^{(\rho_m)} \end{bmatrix} - \begin{bmatrix} L_f^{\rho_1} h_1(x) \\ L_f^{\rho_2} h_2(x) \\ \vdots \\ L_f^{\rho_m} h_m(x) \end{bmatrix} \right) \quad (19)$$

can be used to track a given smooth reference trajectory $y_{\mathrm{ref}}(t)$. This kind of flatness-based control has been applied in the literature in many examples, for instance in motion planning [20], for 2D crane control [1] and for a standard n-trailer system control [21]. In these cases, each control variable has been explicitly determined as function of the desired outputs and their successive derivatives. The expression given in (19) is a compact matrix form of the flatness-based control for a multi-input multi-output system. It is essential to note that u is a function of y_{ref} and its derivatives only, since according to the definition of a flat system, the state x verifies (15). It is therefore a major difference with input-output linearization techniques.

Remark 1. *A necessary condition to include all the dynamics of all the state variables (and therefore be able to express them in terms of the desired outputs and their successive derivatives), is that the sum of the orders of differentiation of the outputs is equal to the order of the system (number of state variables):*

$$\sum_{i=1}^{m} \rho_i = n. \quad (20)$$

In addition, every input has to be associated to a different output.

Remark 2. *One should make sure that the coupling matrix $\Delta(x)$ given in equation (17) is invertible (at least locally). Otherwise, the flatness-based control cannot be used, since the control variables cannot be decoupled, i.e. we will not be able to express each control input independently as function of the desired outputs and their successive derivatives as required for a flatness-based control.*

4.2 Complete state-space model

The state of the platform model can be chosen as $x = [x_1, x_2, x_3, \dots x_7]^\top = [\theta_x, \theta_y, \dot{\theta}_x, \dot{\theta}_y, P_1, P_2, P_3]^\top$, whereas the input vector is $u = [q_1, q_2, q_3]^\top$.

Remark 3. *For the control law synthesis, we have considered the mass flow rates as the input variables instead of the voltages, in order to get an explicit expression of the control*

as will be shown later. The static characteristic of the servovalve will then be inverted numerically to determine the voltage that should be applied. The computation allows getting the required flow rate at any time, and it uses the desired outputs, the pressure inside each muscle from the inversion of the quasi-static model in (7), and the platform dynamics in (6). Note that the required efforts and pressure values for the trajectory tracking can be deduced at any time from the reference.

By neglecting the perturbation term Γ, the system dynamics can then be expressed as follows.

$$\dot{x} = f(x) + g(x)u, \tag{21}$$

where $f(x) =$

$$\left[\begin{array}{c} x_3 \\ \hline x_4 \\ \hline \begin{array}{c} -\cos x_1 \cos x_2 \sin\phi_1 \left(H(\varepsilon_1)(x_5-P_0)+L(\varepsilon_1)\right) \\ -\cos x_1 \cos x_2 \sin\phi_2 \left(H(\varepsilon_2)(x_6-P_0)+L(\varepsilon_2)\right) \\ -\cos x_1 \cos x_2 \sin\phi_3 \left(H(\varepsilon_3)(x_7-P_0)+L(\varepsilon_3)\right) \end{array} \\ \hline \begin{array}{c} (\cos\phi_1 \cos x_2 + \sin\phi_1 \sin x_1 \sin x_2)\left(H(\varepsilon_1)(x_5-P_0)+L(\varepsilon_1)\right) \\ +(\cos\phi_2 \cos x_2 + \sin\phi_2 \sin x_1 \sin x_2)\left(H(\varepsilon_2)(x_6-P_0)+L(\varepsilon_2)\right) \\ +(\cos\phi_3 \cos x_2 + \sin\phi_3 \sin x_1 \sin x_2)\left(H(\varepsilon_3)(x_7-P_0)+L(\varepsilon_3)\right) \end{array} \\ \hline a(\varepsilon_1,\dot{\varepsilon}_1)(x_5-P_0) \\ \hline a(\varepsilon_2,\dot{\varepsilon}_2)(x_6-P_0) \\ \hline a(\varepsilon_3,\dot{\varepsilon}_3)(x_7-P_0) \end{array}\right] \tag{22}$$

$g(x) = [g_1(x), g_2(x), g_3(x)]$ with

$$g_1(x) = \begin{bmatrix} 0 \\ 0 \\ 0 \\ 0 \\ b(\varepsilon_1) \\ 0 \\ 0 \end{bmatrix}, \quad g_2(x) = \begin{bmatrix} 0 \\ 0 \\ 0 \\ 0 \\ 0 \\ b(\varepsilon_2) \\ 0 \end{bmatrix}, \quad g_3(x) = \begin{bmatrix} 0 \\ 0 \\ 0 \\ 0 \\ 0 \\ 0 \\ b(\varepsilon_3) \end{bmatrix} \tag{23}$$

and

$$\begin{cases} a(\varepsilon_i,\dot{\varepsilon}_i) = -\dfrac{k}{V(\varepsilon_i)}\dfrac{\partial V(\varepsilon_i)}{\partial \varepsilon_i}\dot{\varepsilon}_i \\ b(\varepsilon_i) = \dfrac{krT}{V(\varepsilon_i)}. \end{cases} \tag{24}$$

It should noted that the dependency of the right hand side of equation (23) and of both sides of (24) on the state x is omitted for readability reason. According to equation (1), the contractions ε_i are functions of θ_x and θ_y and therefore they are functions of the state x, i.e. $\varepsilon_i = \varepsilon_i(x)$ and $\dot{\varepsilon}_i = \dot{\varepsilon}_i(x)$.

4.3 Flatness of the model

At first, a flat output $[y_1 y_2 y_3]^\top$ has to be determined and it has to be written according to (14), such that equations (15) and (16) hold and the conditions stated in Remarks 1 and 2 are fulfilled.

Let us note that for non-linear systems, there is no general method for determining a flat output and for proving its uniqueness (whereas for linear systems the flat output is unique and easily determined from the Smith form [22] or from the Brunovsky form [20]).

This paragraph shows that the by adopting the following output:

$$\begin{cases} y_1 = x_1 \\ y_2 = x_2 \\ y_3 = F_3 = H(\varepsilon_3)(x_7 - P_0) + L(\varepsilon_3) \end{cases} \tag{25}$$

the system is actually flat.

In order to prove the validity of equation (15), we can remark that x_1, x_2, x_3 and x_4 can be obtained directly from y_1, y_2 and their first time derivatives. Once x_1, x_2, x_3 and x_4 are known, all ε_i, $H(\varepsilon_i)$ and $L(\varepsilon_i)$ are determined as well. Since F_3 is an output and $H(\varepsilon_3) \neq 0$, x_7 is immediately also determined. At last, x_5 and x_6 can be determined from $\dot{x}_3$ and $\dot{x}_4$ if the matrix

$$\begin{bmatrix} -\cos x_1 \cos x_2 \sin\phi_1 & -\cos x_1 \cos x_2 \sin\phi_2 \\ \cos x_2 \cos\phi_1 + \sin x_1 \sin x_2 \sin\phi_1 & \cos x_2 \cos\phi_2 + \sin x_1 \sin x_2 \sin\phi_2 \end{bmatrix}$$

is invertible. The determinant of this matrix is $\cos^2 x_2 \cos x_1 (\sin\phi_2 \cos\phi_1 - \sin\phi_1 \cos\phi_2)$ which is never 0 in the range of $\theta_x = x_1$, $\theta_y = x_2$ allowed for the platform (i.e. they never reach $\pm 90°$).

We now compute the relative degree of each output and their Lie derivatives along the vectors $g_i(x)$ and $f(x)$ for $i \in \{1,2,3\}$. These derivatives will be used to verify equation (20) (Remark 1), the invertibility of $\Delta(x)$ (Remark 2), and for the synthesis of the control law.

Output y_1

$L_{g_1} y_1 = L_{g_2} y_1 = L_{g_3} y_1 = 0 \Rightarrow \rho_1 > 1;$

$L_f y_1 = x_3;$
$L_{g_1} L_f y_1 = L_{g_2} L_f y_1 = L_{g_3} L_f y_1 = 0 \quad \Rightarrow \rho_1 > 2;$

$$\begin{aligned} L_f^2 y_1 &= \dot{x}_3 \\ &= -\cos x_1 \cos x_2 \left(\sin\phi_1 (H(\varepsilon_1)(x_5 - P_0) + L(\varepsilon_1)\right) \\ &\quad + \sin\phi_2 \left(H(\varepsilon_2)(x_6 - P_0) + L(\varepsilon_2)\right) \\ &\quad + \sin\phi_3 \left(H(\varepsilon_3)(x_7 - P_0) + L(\varepsilon_3)\right); \end{aligned}$$

$$L_{g_1}L_f^2 y_1 = -\sin\phi_1 \cos x_1 \cos x_2 H(\varepsilon_1) b(\varepsilon_1),$$
$$L_{g_2}L_f^2 y_1 = -\sin\phi_2 \cos x_1 \cos x_2 H(\varepsilon_2) b(\varepsilon_2),$$
$$L_{g_3}L_f^2 y_1 = -\sin\phi_3 \cos x_1 \cos x_2 H(\varepsilon_3) b(\varepsilon_3).$$

It can be pointed out that $L_{g_1}L_f^2 y_1$, $L_{g_2}L_f^2 y_1$ and $L_{g_3}L_f^2 y_1$ are never equal to 0 for the x_1 and x_2 within the valid range, which makes $\rho_1 = 3$.

Output y_2

$$L_{g_1} y_2 = L_{g_2} y_2 = L_{g_3} y_2 = 0 \Rightarrow \rho_2 > 1;$$

$$L_f y_2 = x_4;$$
$$L_{g_1}L_f y_2 = L_{g_2}L_f y_2 = L_{g_3}L_f y_2 = 0 \Rightarrow \rho_2 > 2;$$

$$\begin{aligned} L_f^2 y_2 &= \dot{x}_4 \\ &= (\cos\phi_1 \cos x_2 + \sin\phi_1 \sin x_1 \sin x_2) \\ &\quad \times (H(\varepsilon_1)(x_5 - P_0) + L(\varepsilon_1)) \\ &\quad + (\cos\phi_2 \cos x_2 + \sin\phi_2 \sin x_1 \sin x_2) \\ &\quad \times (H(\varepsilon_2)(x_6 - P_0) + L(\varepsilon_2)) \\ &\quad + (\cos\phi_3 \cos x_2 + \sin\phi_3 \sin x_1 \sin x_2) \\ &\quad \times (H(\varepsilon_3)(x_7 - P_0) + L(\varepsilon_3)); \end{aligned}$$

$$L_{g_1}L_f^2 y_2 = (\cos\phi_1 \cos x_2 + \sin\phi_1 \sin x_1 \sin x_2) H(\varepsilon_1) b(\varepsilon_1),$$
$$L_{g_2}L_f^2 y_2 = (\cos\phi_2 \cos x_2 + \sin\phi_2 \sin x_1 \sin x_2) H(\varepsilon_2) b(\varepsilon_2),$$
$$L_{g_3}L_f^2 y_2 = (\cos\phi_3 \cos x_2 + \sin\phi_3 \sin x_1 \sin x_2) H(\varepsilon_3) b(\varepsilon_3).$$

Notice that $L_{g_2}L_f^2 y_2$ can never be zero in the valid range, as the function

$$z = \cos\phi_2 \cos x_2 + \sin\phi_2 \sin x_1 \sin x_2 \tag{26}$$

plotted in Fig. 5 never reaches zero in this interval. Thus $\rho_2 = 3$.

Output y_3

$$L_{g_1} y_3 = L_{g_2} y_3 = 0;$$
$$L_{g_3} y_3 = b(\varepsilon_3) H(\varepsilon_3) \neq 0 \Rightarrow \rho_3 = 1.$$

The necessary condition (20) is satisfied as $\rho_1 + \rho_2 + \rho_3 = 7$. Furthermore, one can readily check from the calculation of ρ_i, $i \in \{1,2,3\}$ that every input is associated to a different output. The last step is to verify that the coupling

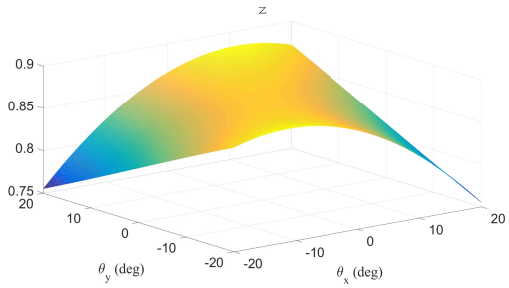

Fig. 5. Value of z as function of $x_1 = \theta_x$ and $x_2 = \theta_y$.

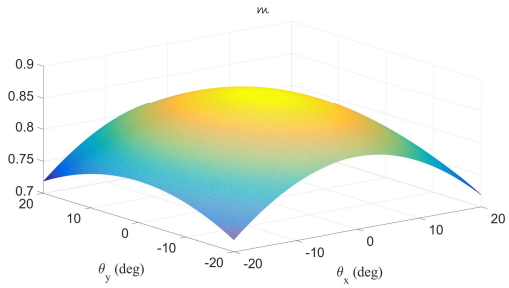

Fig. 6. Values of m as function of θ_x and θ_y.

matrix

$$\Delta = \begin{bmatrix} L_{g_1}L_f^2 y_1 & L_{g_2}L_f^2 y_1 & L_{g_3}L_f^2 y_1 \\ L_{g_1}L_f^2 y_2 & L_{g_2}L_f^2 y_2 & L_{g_3}L_f^2 y_2 \\ L_{g_1} y_3 & L_{g_2} y_3 & L_{g_3} y_3 \end{bmatrix} \tag{27}$$

is invertible. The expression of Δ is made explicit in (28) at the top of the next page (with the shorthand notation of $H_i = H(\varepsilon_i)$, $L_i = L(\varepsilon_i)$, $b_i = b(\varepsilon_i)$).

The determinant of this matrix is $|\Delta| = H_1 H_2 H_3 b_1 b_2 b_3 m$ with $m = -\sin\phi_1 \cos x_1 \cos x_2 (\cos\phi_2 \cos x_2 + \sin\phi_2 \sin x_1 \sin x_2) + \sin\phi_2 \cos x_1 \cos x_2 (\cos\phi_1 \cos x_2 + \sin\phi_1 \sin x_1 \sin x_2)$. The values of m as function of θ_x and θ_y in the valid interval are depicted in Fig. 6

Accordingly, $|\Delta| \neq 0$, and therefore the coupling matrix is invertible over the operating range and the chosen output is proven to be flat.

4.4 Control law

The explicit expression of a flatness-based open-loop control law can now be determined as

$$\begin{bmatrix} \bar{q}_1 \\ \bar{q}_2 \\ \bar{q}_3 \end{bmatrix} = \Delta^{-1}(\bar{x}) \left(\begin{bmatrix} \bar{y}_1^{(\rho_1)} \\ \bar{y}_2^{(\rho_2)} \\ \bar{y}_3^{(\rho_3)} \end{bmatrix} - \begin{bmatrix} L_f^3 \bar{y}_1 \\ L_f^3 \bar{y}_2 \\ L_f \bar{y}_3 \end{bmatrix} \right), \tag{29}$$

$$\Delta = \begin{bmatrix} -\sin\phi_1 \cos x_1 \cos x_2 H_1 b_1 & -\sin\phi_2 \cos x_1 \cos x_2 H_2 b_2 & -\sin\phi_3 \cos x_1 \cos x_2 H_3 b_3 \\ (\cos\phi_1 \cos x_2 + \sin\phi_1 \sin x_1 \sin x_2) H_1 b_1 & (\cos\phi_2 \cos x_2 + \sin\phi_2 \sin x_1 \sin x_2) H_2 b_2 & (\cos\phi_3 \cos x_2 + \sin\phi_3 \sin x_1 \sin x_2) H_3 b_3 \\ 0 & 0 & H_3 b_3 \end{bmatrix} \tag{28}$$

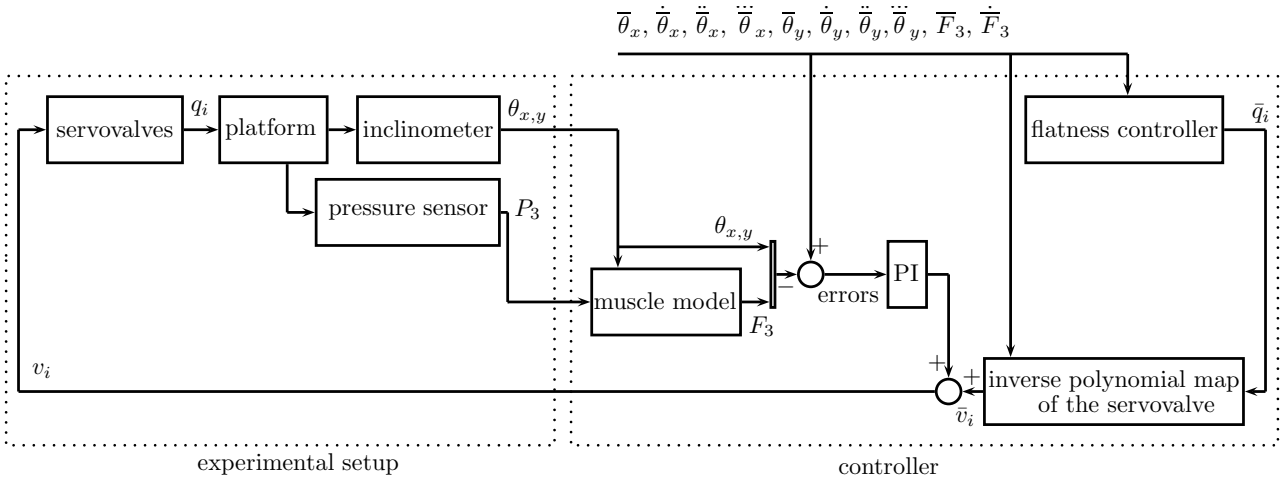

Fig. 7. Global control scheme.

where $\overline{y}_i$ is the reference trajectory; we will denote as well the variables calculated from this reference by an over-line. The voltages $\overline{v_i}$ that should be supplied to the servovalves are computed according to Remark 3. Due to the presence of the perturbation terms (Γ) which have been neglected, there will necessarily be a non-zero error $\varepsilon_i = y_i - \overline{y}_i$. The flatness-based control only provides a feedforward action and therefore it is guaranteed not to destabilise the system; on the other hand, it is not robust to model errors. For this reason, we introduce a feedback term, consisting of a proportional-integral (PI) controller acting in parallel with the flatness-based, open-loop contribution:

$$v_i = \overline{v}_i + k_p \varepsilon_i + k_i \int_0^t \varepsilon_i \, dt. \tag{30}$$

This PI controller provides robustness with respect to modelling errors; its gains have been tuned experimentally (i.e. assuming a linearised model as reference and then improved with trials and errors). A detailed discussion over the overall stability of the system, which should also take into account possible model errors, is out of the scope of this paper. However we can say that stability here is not a concern if the PI is carefully tuned, due to the fact that the dynamics of artificial muscles already has a stabilising effect. Figure 7 shows the overall control scheme. We can notice that the open-loop control contribution is generated without any sensor output, and then added to the PI feedback control which is based on measured errors.

The flatness-based control reveals some common aspects with the feedback linearisation control. [23] The main difference lies in the fact that flatness-based requires a specific choice of flat output, whereas feedback linearisation can take any output, assuming the system is observable, and requires also the knowledge of the state variables.

5 Solving the overactuation

It can be pointed out that the platform is overactuated, in the sense that the three forces applied by the muscles are generating only two torques. To tell it in another way, the average value of the F_i is irrelevant for the platform's dynamics; if a given $F_1 = \tilde{F}_1$, $F_2 = \tilde{F}_2$ and $F_3 = \tilde{F}_3$ generate certain torques, then $F_1 = \tilde{F}_1 + F_0$, $F_2 = \tilde{F}_2 + F_0$ and $F_3 = \tilde{F}_3 + F_0$ will generate the same torques for any F_0. Nevertheless, it is required to have three muscles instead of two due to the fact that muscles can only pull and not push, i.e. their force range is limited to positive values as shown by Fig. 3.

On the other hand, a given position of the platform cor-

responds to three values of the contractions ε_i; so the effort exerted by each muscle at that position, according to Fig. 3, is bounded to be between a maximal value $F_{i,max}$ and a minimal value $F_{i,min}$. These limit values depend of course on ε_i and on the fact that the range of the allowed pressures is between 1.25 and 7 bar. Consequently, we can compute the maximum and the minimum allowed forces that can be exerted by any of the three muscles at any given position by

$$F_{max} = \min_{i\in\{1,2,3\}} (F_{i,max}), \tag{31}$$

$$F_{min} = \max_{i\in\{1,2,3\}} (F_{i,min}), \tag{32}$$

as depicted in Fig. 8. The operating range associated to a platform position defined by ε_1, ε_2 and ε_3 is marked by the shaded area. The reference trajectories $\bar{\theta}_x$ and $\bar{\theta}_y$ can be defined according to a desired movement for the platform, whereas the reference trajectory $\bar{F}_3$ can be chosen in order to satisfy other objectives or constraints. The flat control allows choosing the value of F_3, which lets one make the best choice in order to let all the muscles stay in their operating force range. Roughly speaking, increasing the desired value of F_3 will add some stiffness to the system, since more pressure will be supplied into the muscles in order to have the required position, whereas decreasing the value of F_3 will add more compliance.

Under the reasonable hypothesis that the platform moves slowly (in any case it is constrained to angles smaller than 15°), it can be assumed that F_1, F_2 and F_3 have to be close to the equilibrium values, i.e. $F_1 \approx F_2 \approx F_3$. For this reason, setting the reference for F_3 as

$$\bar{F}_3 = \frac{1}{2}(F_{max}(\bar{\varepsilon}_1,\bar{\varepsilon}_2,\bar{\varepsilon}_3) + F_{min}(\bar{\varepsilon}_1,\bar{\varepsilon}_2,\bar{\varepsilon}_3)) \tag{33}$$

with $\bar{\varepsilon}_i = \bar{\varepsilon}_i(\bar{\theta}_x,\bar{\theta}_y)$, will make F_1 and F_2 within the allowed interval as well, and therefore all the efforts will definitely belong to the operating range at equal distance from its boundaries. Note that the reference trajectory $\bar{F}_3$ can be determined offline from the reference trajectories $\bar{\theta}_x$ and $\bar{\theta}_y$ using (33).

6 Some considerations on sliding mode control

As mentionnend in the introduction, the vast majority of the literature concerning the control of pneumatic artificial muscles makes use of sliding mode control [6, 7, 8]. Sliding mode is a very attractive choice, because of its inherent robustness and ease of tuning. Nevertheless, it works by alternating very strong control actions in opposite directions, resulting in the so-called chattering phenomenon, i.e. small

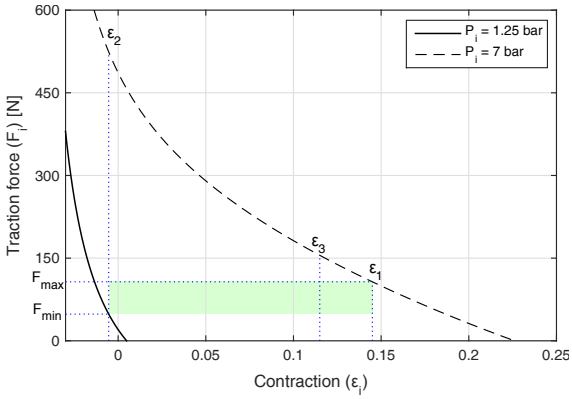

Fig. 8. Valid range of the efforts, bounded from below by F_{min} and from above by F_{max} for a given position of the platform, determined by the three contractions ε_i, $i \in \{1,2,3\}$.

oscillations around the reference trajectory. Even if such oscillations might be small, in mechanical systems they will produce vibrations (high frequency actions on the components) as well as noise, both highly undesirable. For the sake of clarity, we have designed a sliding mode controller to our system by constructing a sliding surface in the sense of [8], the error being on the three output components. The detailed calculations are out of the scope of this paper and so they are not reported here. Fig. 9 shows the value of the force F_3 during a simulated experiment involving trajectory tracking. The figure clearly shows a chattering phenomenon; such a phenomenon can be attenuated by adding a boundary layer thickness to the standard sign function. However, the effect will persist with just vibrations of smaller amplitude. This phenomenon is instead totally absent if flatness-based control is used.

Another drawback of the sliding mode is that, due to the high relative degree of the output (equal to 3 for θ_x and θ_y), the feedback control requires computing the second derivative of the measured angles, which is numerically problematic. This can be achieved by either using online derivatives of the output signals or designing a non-linear state observer that yields the computation of $\ddot{\theta}_x$ and $\ddot{\theta}_y$. Either way, this makes the control implementation more cumbersome. On the other hand, by using the flatness-based control, the derivatives of the output signals are not required since this approach is an open-loop control and it relies on offline computations using the reference and its derivatives.

7 Experimental results

A set of experiments has been conducted on the platform in order to assess the performance of the proposed control approach. The sampling time is 0.01 s and the inclinometers' output has a quantisation of 0.18 degrees. We remind

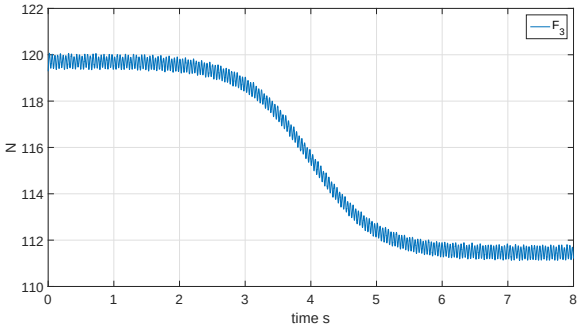

Fig. 9. Simulation result of the evolution of the output F_3 when the sliding mode control is used.

the reader that the trajectories assigned to θ_x and θ_y have to be smooth enough (at least three times differentiable) so that the control can be computed according to (29). Let us first consider a smooth step described by the hyperbolic tangent function to check the precision in reaching a final static position. The target angles for θ_x and θ_y are chosen to be $+6$ and -6 degrees respectively, so that the muscles operate at a wide range. Fig. 10 shows that the measured response (inclinometer output) of the platform converges instantly to the desired trajectories for θ_x and θ_y. The plots of the contractions are depicted in Fig. 11, where the actual contractions, reconstructed from the output angles using (1), are compared with the reference. As we can notice, these plots highlight a considerable operating range of the muscles (0 to 0.124% contraction) including the non-linear region illustrated in Fig. 3.

Next, the proposed flatness-based control coupled with a PI controller is compared with a PI controller, empirically tuned to get the best apparent performances (the scheme can be obtained from Fig. 7 by omitting the feed-forward control part). We apply as reference a combination of sinusoids, representing a generalization of any dynamic smooth variations. We should note that the parameters of the proportional and integral contributions, as well as the reference trajectory, have been kept the same for both controllers during the test. Figure 12 reports the results for the PI controller, whereas Fig. 13 shows the flatness-based controller results. It is clear from Fig. 12 and 13 that the feedforward action added by the flatness-based control greatly improves the tracking ability. The root mean square tracking errors (for θ_x and θ_y respectively) are 0.51 and 0.59 degrees with the PI controller, whereas it is less than 0.25 and 0.29 degrees respectively with the flatness controller. We notice as well a better trajectory tracking when the flatness-based control is used, especially in terms of delay with respect to the reference trajectory.

Figures 14 and 15 show the evolution of the pressures

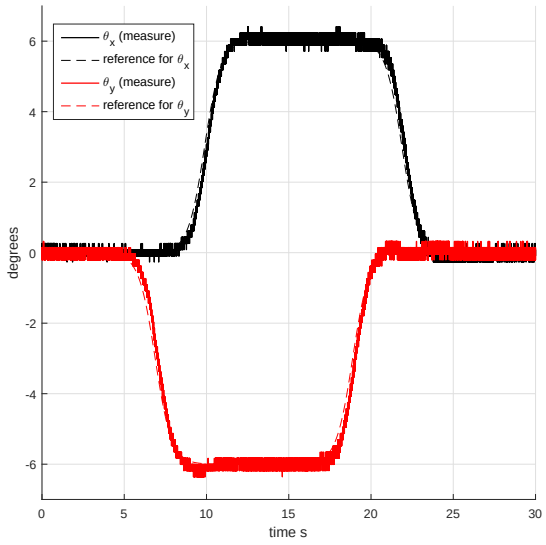

Fig. 10. Static set point tracking using the flatness-based control plus a PI.

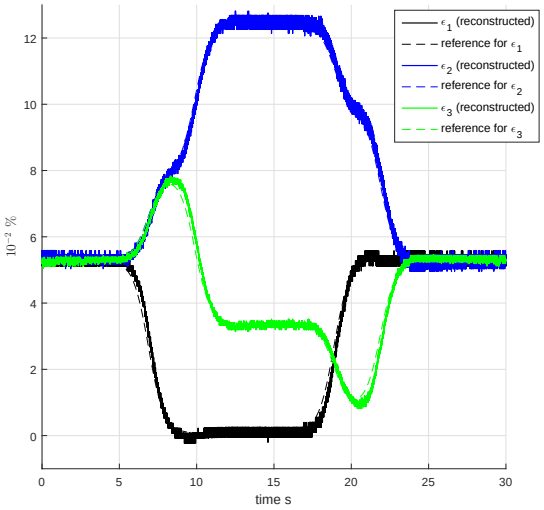

Fig. 11. Muscles contraction for the setpoint tracking.

and the forces exerted by the three muscles respectively during the flatness-based controller test. Note that the reference $\bar{F}_3$ is determined by the overactuation-solving law (33). Interestingly, the forces never saturate (and neither do the voltages nor the pressures), which validates the proposed strategy.

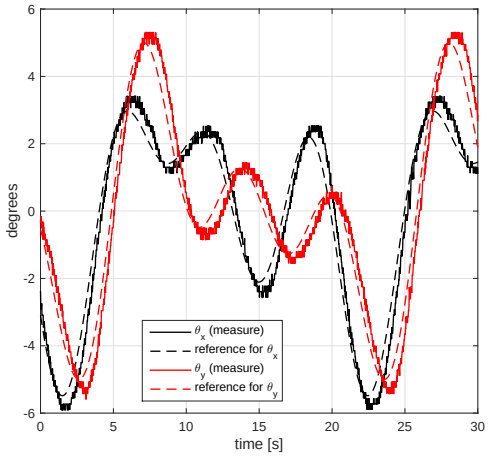

Fig. 12. Trajectory tracking with simple PI control.

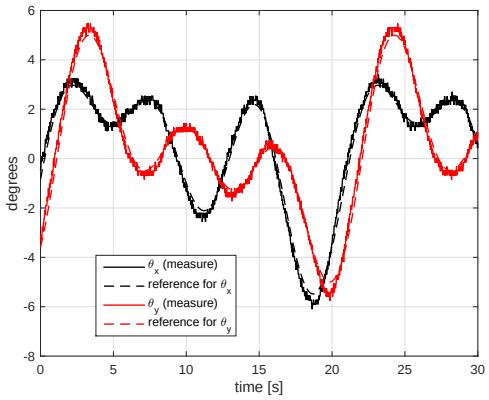

Fig. 13. Trajectory tracking with flatness-based control plus a PI.

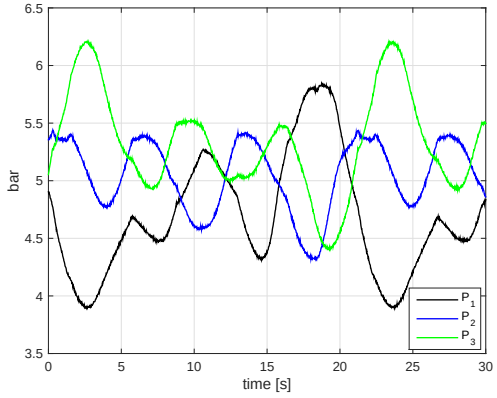

Fig. 14. Pressures inside the pneumatic artificial muscles during the flatness-based control plus PI experiment.

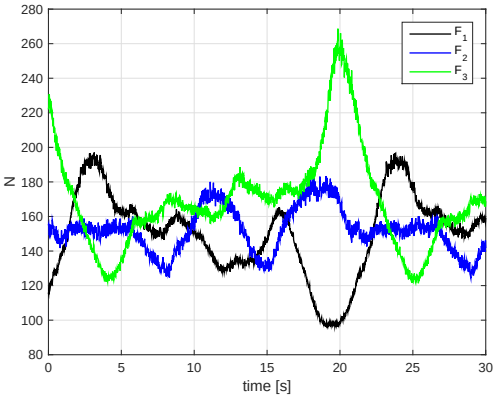

Fig. 15. Forces applied by the pneumatic artificial muscles (estimated using (6) and the measurements of the pressures and the contractions) with flatness-based control plus a PI.

8 Conclusion

This paper has presented a successful application of a flatness-based control (a non-linear open-loop control) augmented with a PI controller to a platform featuring three PAMs and presenting an overactuation. We have shown that by choosing an adequate output the system is flat, and that a flatness-based controller can be computed based on the inverse of a coupling matrix. The control law, consisting of the mass flow rates applied to the muscles, is explicitly expressed in terms of the desired output and its successive derivatives. The required voltages are consequently calculated by a numerical inversion of the static characteristic of the servovalve. The platform features an overactuation, which is solved by an appropriate choice of the third output component, restraining the muscles efforts to their valid operating range. The flatness-based controller, being applied in open-loop, does not require any state or output feedback; however, in order to compensate any model error and perturbations, a PI controller is added.

The experimental results clearly show a better trajectory tracking compared to a simple PI controller, highlighting the relevancy of a non-linear model-based control for systems accurately modeled. Interestingly, the control performance is independent from the shape of the trajectory itself. We showed its efficiency in moving the platforma to a static setpoint, as well as in tracking dynamical variations in a wide operating range of the muscles.

Compared to a sliding mode control, the flatness-based approach provides a good level of performance with no chattering, which usually causes undesirable high-frequency vibrations and noise. In addition, whereas other non-linear controllers for this system will require the knowledge of high order derivatives of the platform position in the feedback loop, the flatness-based control law is expressed offline only

as function of the desired output and its successive derivatives. This can significantly simplify the implementation of a non-linear controller. Based on this, we conclude that the proposed approach yields a reliable controller providing a good tracking accuracy.

Future research will look at the possibility of using PAMs for building a complete six-degree-of-freedom Stewart platform, and controlling it with the same approach.

References

[1] Fliess, M., Lévine, J., Martin, P., and Rouchon, P., 1995. "Flatness and defect of non-linear systems: introductory theory and examples". *International Journal of Control*, **61**(6), pp. 1327–1361.

[2] Daerden, F., and Lefeber, D., 2002. "Pneumatic artificial muscles: actuators for robotics and automation". *European journal of mechanical and environmental engineering*, **47**(1), pp. 11–21.

[3] Shen, W., and Shi, G., 2011. "An enhanced static mathematical model of braided fibre-reinforced pneumatic artificial muscles". *Proceedings of the Institution of Mechanical Engineers, Part I: Journal of Systems and Control Engineering*, **225**(2), pp. 212–225.

[4] Ba, D., Dinh, T., and Ahn, K., 2016. "An integrated intelligent nonlinear control method for a pneumatic artificial muscle". *IEEE/ASME Transactions on Mechatronics*, **21**(4), pp. 1835–1845.

[5] Zhu, X., Tao, G., Yao, B., and Cao, J., 2008. "Adaptive robust posture control of parallel manipulator driven by pneumatic muscles with redundancy". *IEEE/ASME Transactions on Mechatronics*, **13**(4), August, pp. 441–450.

[6] Aschemann, H., and Schindele, D., 2008. "Sliding-mode control of a high-speed linear axis driven by pneumatic muscle actuators". *IEEE Transactions on Industrial Electronics*, **55**(11), pp. 3855–3864.

[7] Cai, D., and Dai, Y., 2000. "A sliding mode controller for manipulator driven by artificial muscle actuator". In Proceedings of the 2000 IEEE International Conference on Control Applications, IEEE, pp. 668–673.

[8] Shen, X., 2010. "Nonlinear model-based control of pneumatic artificial muscle servo systems". *Control Engineering Practice*, **18**(3), pp. 311–317.

[9] Ahn, K., and Anh, H., 2007. "A new approach for modelling and identification of the pneumatic artificial muscle manipulator based on recurrent neural networks". *Proceedings of the Institution of Mechanical Engineers, Part I: Journal of Systems and Control Engineering*, **221**(8), pp. 1101–1121.

[10] Shi, G., and Shen, W., 2013. "Hybrid control of a parallel platform based on pneumatic artificial muscles combining sliding mode controller and adaptive fuzzy CMAC". *Control Engineering Practice*, **1**(1), pp. 76–86.

[11] Robinson, R., Kothera, C., Sanner, R., and Wereley, N., 2016. "Nonlinear control of robotic manipulators driven by pneumatic artificial muscles". *IEEE/ASME Transactions on Mechatronics*, **21**(1), February, pp. 55–68.

[12] Rahman, R., and Sepehri, N., 2016. "Design and experimental evaluation of a dynamical adaptive backstepping-sliding mode control scheme for positioning of an antagonistically paired pneumatic artificial muscles driven actuating system". *International Journal of Control*, pp. 1–26.

[13] Chou, C.-P., and Hannaford, B., 1996. "Measurement and modeling of McKibben pneumatic artificial muscles". *IEEE Transactions on Robotics and Automation*, **12**(1), pp. 90–102.

[14] Tondu, B., and Lopez, P., 2000. "Modeling and control of McKibben artificial muscle robot actuators". *Control Systems, IEEE*, **20**(2), pp. 15–38.

[15] Sermeno Mena, S., Sesmat, S., and Bideaux, E., 2012. "Parallel manipulator driven by pneumatic muscles". In 8th International Conference on Fluid Power (8th IFK) 2012.

[16] Schindele, D., and Aschemann, H., 2012. "Model-based compensation of hysteresis in the force characteristic of pneumatic muscles". In Advanced Motion Control (AMC), 2012 12th IEEE International Workshop on, IEEE, pp. 1–6.

[17] Bou Saba, D., Bideaux, E., Brun, X., and Massioni, P. "A complete model of a two degree of freedom platform actuated by three pneumatic muscles elaborated for control synthesis". In BATH/ASME 2016 Symposium on Fluid Power and Motion Control.

[18] Olaby, O., Brun, X., Sesmat, S., Redarce, T., and Bideaux, E., 2005. "Characterization and modeling of a proportional valve for control synthesis". In Proceedings of the JFPS International Symposium on Fluid Power, Vol. 2005, The Japan Fluid Power System Society, pp. 771–776.

[19] Rouchon, P., 2005. "Flatness based control of oscillators". *ZAMM-Journal of Applied Mathematics and Mechanics/Zeitschrift für Angewandte Mathematik und Mechanik*, **85**(6), pp. 411–421.

[20] Martin, P., Murray, R. M., and Rouchon, P., 2003. "Flat systems, equivalence and trajectory generation".

[21] Rouchon, P., Fliess, M., Lévine, J., and Martin, P., 1993. "Flatness, motion planning and trailer systems". In Decision and Control, 1993., Proceedings of the 32nd IEEE Conference on, IEEE, pp. 2700–2705.

[22] Lévine, J., and Nguyen, D., 2003. "Flat output characterization for linear systems using polynomial matrices". *Systems & control letters*, **48**(1), pp. 69–75.

[23] Isidori, A., 2013. *Nonlinear control systems*. Springer Science & Business Media.